STEM CELLS®

TISSUE-SPECIFIC STEM CELLS

Mesenchymal Stem Cells Transmigrate Between and Directly Through Tumor Necrosis Factor-α-Activated Endothelial Cells via Both Leukocyte-Like and Novel Mechanisms

GRACE S. L. TEO,[a,b] JAMES A. ANKRUM,[a] ROBERTA MARTINELLI,[b] SARAH E. BOETTO,[a] KAYLA SIMMS,[a] TRACEY E. SCIUTO,[b] ANN M. DVORAK,[b] JEFFREY M. KARP,[a] CHRISTOPHER V. CARMAN[b]

[a]Division of Biomedical Engineering, Department of Medicine, Center for Regenerative Therapeutics, Brigham and Women's Hospital, Harvard Medical School, Harvard Stem Cell Institute, Harvard-MIT Division of Health Sciences and Technology, Cambridge, Massachusetts, USA; [b]Beth Israel Deaconess Medical Center, Center for Vascular Biology, Harvard Medical School, Boston, Massachusetts, USA

Key Words. Diapedesis • Mesenchymal stem cell • Cell migration • Inflammation • Bleb • Adhesion

ABSTRACT

Systemically administered adult mesenchymal stem cells (MSCs), which are being explored in clinical trials to treat inflammatory disease, exhibit the critical ability to extravasate at sites of inflammation. We aimed to characterize the basic cellular processes mediating this extravasation and compare them to those involved in leukocyte transmigration. Using high-resolution confocal and dynamic microscopy, we show that, like leukocytes, human bone marrow-derived MSC preferentially adhere to and migrate across tumor necrosis factor-α-activated endothelium in a vascular cell adhesion molecule-1 (VCAM-1) and G-protein-coupled receptor signaling-dependent manner. As several studies have suggested, we observed that a fraction of MSC was integrated into endothelium. In addition, we observed two modes of transmigration not previously observed for MSC: Paracellular (between endothelial cells) and transcellular (directly through individual endothelial cells) diapedesis through discrete gaps and pores in the endothelial monolayer, in association with VCAM-1-enriched "transmigratory cups". Contrasting leukocytes, MSC transmigration was not preceded by significant lateral migration and occurred on the time scale of hours rather than minutes. Interestingly, rather than lamellipodia and invadosomes, MSC exhibited nonapoptotic membrane blebbing activity that was similar to activities previously described for metastatic tumor and embryonic germ cells. Our studies suggest that low avidity binding between endothelium and MSC may grant a permissive environment for MSC blebbing. MSC blebbing was associated with early stages of transmigration, in which blebs could exert forces on underlying endothelial cells indicating potential functioning in breaching the endothelium. Collectively, our data suggest that MSC transmigrate actively into inflamed tissues via both leukocyte-like and novel mechanisms. STEM CELLS *2012;30:2472–2486*

Disclosure of potential conflicts of interest is found at the end of this article.

INTRODUCTION

More than 100 clinical trials currently evaluate adult "mesenchymal stem cells" (MSCs) or "multipotent stromal cells" for treatment of diverse inflammatory, cardiovascular, and autoimmune diseases [1]. Approximately half of the clinical trials involve the systemic infusion of MSC into the vascular circulation [1]. Preclinical animal studies demonstrate that infused MSC preferentially engraft into inflamed or ischemic tissues, a behavior that is thought to be critical for their therapeutic efficacy [2]. Additionally, physiological homing ability of endogenous MSC is supported by studies reporting that endogenous MSC can be mobilized from the bone marrow and recruited into wounds [3], tumors [4], ectopic endometrial tissue in endometriosis [5, 6], and sites of intimal hyperplasia [7]. A critical step in such recruitment and engraftment is the exit of MSC from the vascular circulation (i.e., extravasation), which requires crossing the endothelial cell (EC) barrier that lines blood vessels. For MSC, this process of extravasation remains incompletely understood.

Author contributions: G.S.L.T.: conception and design, collection and/or assembly of data, data analysis and interpretation, and manuscript writing; J.A.A. and R.M.: conception and design, collection and/or assembly of data, and data analysis and interpretation; S.E.B. and K.S.: collection and/or assembly of data; T.E.S.: collection and/or assembly of data and data analysis and interpretation; A.M.D.: data analysis and interpretation; J.M.K.: conception and design, financial support, data analysis and interpretation, and manuscript writing; C.V.C.: conception and design, financial support, collection and/or assembly of data, data analysis and interpretation, manuscript writing, and final approval of manuscript.

Correspondence: Jeffrey M. Karp, Ph.D., Division of Biomedical Engineering, Department of Medicine, Center for Regenerative Therapeutics, Brigham and Women's Hospital, Harvard Medical School, Harvard Stem Cell Institute, Harvard-MIT Division of Health Sciences and Technology, Cambridge, Massachusetts, USA. Telephone: 617-817-9174; Fax: 617-768-8338; e-mail: jkarp@rics.bwh.harvard.edu; or Christopher V. Carman, Ph.D., Beth Israel Deaconess Medical Center, Center for Vascular Biology, Harvard Medical School, 330 Brookline Ave., RN-234, Boston, Massachusetts 02215, USA. Telephone: 617-667-0888; Fax: 617-667-2913; e-mail: ccarman@bidmc.harvard.edu Received December 7, 2011; accepted for publication July 17, 2012; first published online in STEM CELLS *EXPRESS* August 7, 2012. 1066-5099/2012/$30.00/0 doi: 10.1002/stem.1198

In contrast, the process of leukocyte extravasation at sites of inflammation has been well-characterized as a dynamic and rapid (time scale of minutes) multistep cascade (Fig. 6). During inflammation, endothelium becomes activated by cytokines such as tumor necrosis factor-α (TNF-α). They then upregulate chemoattractants and surface proteins, including selectins and cell adhesion molecules (CAMs), which mediate rolling and adhesive interactions, respectively. Subsequently, leukocytes initiate a phase of lateral migration over the luminal surface and use dynamic cytoskeletal protrusions (e.g., lamellipodia, pseudopods, and invadosomes) to cross the endothelium through discrete gaps in intercellular junctions (i.e., "paracellular diapedesis") or directly through pores in individual ECs (i.e., "transcellular diapedesis") [8–10]. In parallel, endothelium proactively generates its own actin-dependent protrusions (i.e., "transmigratory cups") that embrace the leukocytes and guide their transmigration [10].

Like leukocytes, previous studies suggest that MSC may also be able to undergo selectin-mediated rolling [11] and integrin-mediated adhesion [11, 12] preferentially on cytokine-activated endothelium. However, unlike leukocytes, a limited number of studies attempting to investigate the cellular process of MSC transmigration have largely suggested an "integration"-based mode of transmigration. MSC integration has been described as the process in which gross-scale retraction of ECs allows for MSC spreading and incorporation into the endothelial monolayer, before the endothelial monolayer ultimately reforms over the integrated MSC [13–15]. However, the molecular and cellular details of this process have not been well-resolved. For example, critical aspects such as detailed three-dimensional (3D) cellular architecture, distribution of adhesion and endothelial junction molecules, and dynamics have not yet been carefully investigated.

We therefore used high-resolution confocal and dynamic live-cell imaging in this study and found strikingly that, in addition to integration, MSC can transmigrate through discrete pores and gaps in the endothelium by paracellular and transcellular diapedesis, in association with endothelial transmigratory cups similarly to leukocytes. However, contrasting leukocytes, MSC transmigration does not involve significant lateral migration, lamellipodia, or invadosomes in the initiation of transmigration. Instead, like some embryonic germ and metastatic tumor cells [16–18], MSCs exhibit nonapoptotic blebbing that can exert forces on ECs during early stages of transmigration.

Materials and Methods

Antibodies and Reagents

The following antibodies were used for immunocytochemistry: IC1/12-Cy3 and IC1/13-Cy3 were as described [19]. ToPro3, Phalloidin-546 and 647, and Cholera toxin B-488 and 546 were from Invitrogen (Carlsbad, CA, www.invitrogen.com). Purified mouse anti-human CD90 (clone 5E10), FITC mouse anti-human CD90 (clone 5E10), and mouse anti-human CD144 (VE-cadherin; clone 55-7H1) were from BD Pharmingen (San Diego, CA, www.bdbiosciences.com). Polyclonal sheep anti-human vascular CAM (VCAM-1) and rabbit anti-human junctional adhesion molecule-1 (JAM-1) were from R&D Systems (Minneapolis, MN, www.rndsystems.com). Purified goat anti-rat VE-Cadherin (sc-6458) and mouse anti-rat ICAM-1 (clone 1A29) were from Santa Cruz (Santa Cruz, CA, www.scbt.com) and Abd Serotec (Raleigh, NC, www.abdserotec.com), respectively. Rabbit polyclonal anti-human occludin was from Abcam (Cambridge, MA, www.abcam.com). Mouse anti-human β-catenin conjugated to Alexa Fluor 647 was from Cell Signaling Technology. Annexin V conjugated to Alexa Fluor 647 was from Molecular Probes (Eugene, OR, www.invitrogen.com). Antibody conjugation to Alexa488, Alexa546, or Alexa647 bisfunctional dyes (Molecular Probes Eugene, OR, www.invitrogen.com) was performed according to manufacturer's instructions. The fluorescent lipophilic dyes, DiI and DiO, were from Invitrogen (Carlsbad, CA, www.invitrogen.com) and used according to the manufacturer's instructions. The following antibodies were used for function-blocking experiments: polyclonal sheep anti-human VCAM-1 (R&D Systems, Minneapolis, MN, www.rndsystems.com), mouse anti-human alpha 4 integrin (HP2/1; Millipore, Billerica, MA, www.millipore.com), sheep IgG isotype control (Jackson Labs, Bar Harbor, Maine, www.jax.org), and mouse IgG1 isotype control (BD, San Diego, CA, www.bdbiosciences.com). The following antibodies were used for flow cytometry analysis of microvascular ECs (MVECs) or GPNTs: AlexaFluor488-conjugated mouse anti-human CD54 (clone RR1/1) (generous gift from Timothy Springer), FITC-conjugated mouse IgG1 isotype control (clone P3.6.2.8.1; eBioscience, San Diego, CA), phycoerythrin (PE)-conjugated mouse anti-human CD106 (clone 51-10C9, BD, San Diego, CA, www.bdbiosciences.com), PE-conjugated mouse IgG1 isotype control (BD, San Diego, CA), mouse anti-rat CD54 (clone IA29, AbD Serotec, Oxford, UK, www.abdserotec.com), mouse anti-rat (CD10, clone 5F10), rat IgG2A isotype control (clone eBR2a, eBioScience, San Diego, CA, www.ebioscience.com), and FITC-conjugated goat anti-mouse secondary antibody (Invitrogen, Carlsbad, CA, www.invitrogen.com). The following antibodies were used for flow cytometry analysis of MSCs and CD4+ T cells: mouse anti-human alpha 4 integrin (HP2/1, Millipore Billerica, MA, www.millipore.com), AlexaFluor488-conjugated mouse anti-human alpha 4 integrin (7.2R, R&D Systems, Minneapolis, MN, www.rndsystems.com), mouse anti-human alpha 5 integrin (MAB1956Z, Millipore, Billerica, MA, www.millipore.com), mouse anti-human beta 1 integrin (P4C10, Millipore, Billerica, MA, www.millipore.com), mouse anti-human beta 2 integrin (TS1/18, gift from Professor Timothy Springer), and murine IgG1 isotype control (ICIGG1, Abcam, Cambridge, MA, www.abcam.com).

MSC Culture

Primary human MSC were obtained isolated from the iliac crest of the hip bone of healthy consenting donors and obtained from the Texas A&M Health Science Center, College of Medicine, Institute for Regenerative Medicine at Scott & White Hospital (Temple, TX). The donor inclusion criteria were that they must be normal, healthy adults, at least 18 years of age, with a normal body mass index and free of infectious diseases (as determined by the blood sample screening performed 1 week before bone marrow donation). In these studies, MSCs from four different donors were used. MSCs were maintained in α-minimum expansion media (α-MEM; Invitrogen, Carlsbad, CA, www.invitrogen.com) supplemented with 15% fetal bovine serum (Atlanta Biologicals, Lawrenceville, GA), 1% L-Glutamine (Invitrogen, Carlsbad, CA, www.invitrogen.com), and 1% Penn-Strep (Invitrogen, Carlsbad, CA, www.invitrogen.com). Cells were cultured to 80% confluence before passaging. All experiments were performed using MSC at passages 3–7 during which they expressed high levels of the MSC markers CD90 and CD29 (>99% cells) and did not express hematopoietic markers CD34 or CD45 (0% of cells), as determined by flow cytometry analysis [20]. MSC senescence at P3, P5, and P7 was assessed using the Senescence β-Galactosidase Staining Kit from Cell Signaling Technology (Danvers, MA), according to manufacturer's instructions. In some cases, MSCs were pretreated with 2.5 μM etoposide for 24 hours followed by drug washout and an additional 72 hours of culture in complete media to induce apoptosis. Stained MSCs were imaged using a Nikon TE2000E inverted microscope (Nikon Instruments, Melville, NY, www.nikoninstruments.com) equipped with a $\times 20$ bright-field objective, CCD camera and NIS Element software

(Melville, NY, www.nis-elements.com). Five microscopic fields of view (each containing at least 50 MSC in total) were captured and the percentage of total MSCs in each field that were senescent (i.e., showed blue colored β-Galactosidase reaction product) was calculated and averaged among the five fields for each condition.

EC Culture

Primary adult human lung (hLMVEC) and cardiac (hCMVEC) microvascular endothelial cells (MVECs) were purchased from Lonza (Basel, CH, www.lonza.com) and cultured on human purified fibronectin (Invitrogen)-coated substrates in EBM-2MV media (Lonza) and used at passages 4–6. Five micrograms of fibronectin per square centimeter was used for coating substrates. The immortalized Lewis rat brain MVEC line Gareth Pryce Newly Transformed (GPNT) was obtained from Dr. John Greenwood (University College of London, U.K.), characterized as described [21, 22] and cultured on collagen-IV-coated substrates (7 μg of collagen per square centimeter) in media composed of a 1:1 ratio of F10 (Invitrogen, Carlsbad, CA, www.invitrogen.com) and α-MEM (Invitrogen) supplemented with 10% fetal bovine serum and 1% Penn-Step. Aortic adventitial fibroblasts were obtained from Lonza (Basel, CH, www.lonza.com) and cultured in Dulbecco's Modified Eagle's medium (Invitrogen, Carlsbad, CA, www.invitrogen.com), supplemented with 10% fetal bovine serum and 1% Penn-Strep. Fibroblasts were used at passages 4–6.

Flow Cytometry

MSC and EC cultures were detached with 0.05% Trypsin-EDTA (Sigma, St. Louis, MO, www.sigmaaldrich.com) and suspended in fluorescence-activated cell sorting buffer (phosphate buffered saline [PBS] containing 2% fetal calf serum, 2 mM EDTA, and 0.03% azide) and then incubated with primary antibodies (10 μg/ml) at 4°C for 30 minutes. Samples were washed three times with PBS, incubated with secondary antibodies, then rewashed and analyzed using a C6 Flow Cytometer (BD Accuri, Ann Arbor, MI, www.bdbiosciences.com) and CFlow software. ECs were either resting or activated by pretreatment with recombinant human TNF-α (50 ng/ml for 16 hours; Peprotech, Rocky Hill, NJ, or Invitrogen, Carlsbad, CA, www.invitrogen.com) and/or IFN-γ (100 ng/ml for 48 hours; Invitrogen, Carlsbad, CA, www.invitrogen.com). For apoptosis studies, MSC, EC, or coincubated MSC and EC were detached from tissue culture plates with 0.05% Trypsin/EDTA and stained with Annexin V and propidium iodide (PI) using the Annexin V/Dead Cell Apoptosis Kit (Invitrogen, Carlsbad, CA, www.invitrogen.com) according to manufacturer's instructions and then analyzed by flow cytometry. In some cases of MSC-EC coincubation, coincubation time was 1 hour and costaining with CD90-647 was used to distinguish MSC from EC. As indicated in some cases, MSCs were pretreated with 100 ng/ml pertussis toxin (PTX) or 1 mM hydrogen peroxide (H_2O_2) for 2 hours.

Fixed-End Point Microscopic Analysis of MSC Adhesion and Transmigration

ECs were plated at 90% confluence in 24-well plates (100,000 cells per 24 well) containing circular coverglass (12-mm diameter) coated with fibronectin (5 μg/cm^2; or for GPNTs, collagen IV at 7 μg/cm^2). These were cultured for 48–72 hours and, as indicated, preactivated for 16 hours with TNF-α (50 ng/ml; Peprotech, Rocky Hill, NJ, www.peprotech.com or Invitrogen, Carlsbad, CA, www.invitrogen.com) or for 48 hours with IFN-γ (100 ng/ml; Invitrogen). Cultured MSCs were detached using 0.05% Trypsin/EDTA (Invitrogen, Carlsbad, CA, www.invitrogen.com), resuspended in EBM-2MV media, added to the EC monolayers, and incubated at 37°C and 5% CO_2 for indicated and then fixed with 3.7% formaldehyde. In some cases, EC and/or MSC were prelabeled with membrane dyes DiI and DiO (1 μg/ml), respectively, for 30 minutes at 37°C, prior to coincubation. As indicated in some cases, ECs were preincubated with blocking anti-VCAM-1 antibody (20 μg/ml; R&D Systems, Minneapolis, MN, www.rndsystems.com) for 30 minutes at 37°C and MSCs were treated with PTX (100 ng/ml; Sigma-Aldrich, St. Louis, MO, www.sigmaaldrich.com) for 2 hours at 37°C.

In the case of prelabeled (i.e., with DiI and DiO samples), imaging was performed directly. For all other experiments (except anti-occludin staining), fixed samples were blocked with 5% non-fat dry milk in PBS (Invitrogen, Carlsbad, CA, www.invitrogen.com) for 5 minutes, variously stained for CD90 (anti-human CD90-488, -546), GM1 gangliosides (an alternate MSC marker; CTx-B-488, 546), VCAM-1 (polyclonal anti-VCAM-1-Cy3), ICAM-1 (ICAM-1-Cy5), F-actin (phalloidin-647), nucleus (ToPro3), VE-cadherin (anti-human-VE-cadherin-Cy5; anti-rat-VE-cadherin-488), and JAM-1 (anti-human-JAM-1-Cy3) in blocking buffer containing 0.05% Triton X-100 for 30 minutes and then washed three times. Anti-occludin staining was performed as previously described [23, 24]. Confocal imaging was conducted on a Zeiss LSM 510 (Zeiss, Heidelberg, DE, www.zeiss.com) using a $\times$63 water immersion objective. For serial Z-stacks, the section thickness ranged from 0.5 to 1.0 μm. 3D reconstruction and projection of Z-stacks were performed with AxioVision software (Zeiss, Heidelberg, DE, www.zeiss.com). The stages of MSC transmigration were determined from the relative distribution of VCAM-1 or ICAM-1 (used as surface marker for ECs), CD90 or CTx-B (used as surface markers for MSC), and actin (to determine structure of both cells) fluorescence in both the *x-y* and *z* dimensions using confocal microscopy as described [19]. Five distinct stages in MSC transmigration were defined and interpreted: (a) MSC adherence to the apical surface of endothelium, (b) endothelial cup formation, (c) endothelial gap/pore formation (initiation of transmigration), (d) subendothelial spreading of the MSC (advanced progression of transmigration), and (e) barrier restoration (MSC is completely on the basal endothelial surface). For some analyses, these stages were collapsed into three major positions of MSC relative to EC: apical (stages 1–2; MSC is completely on the apical side of the EC monolayer); transmigrating (stages 3–4; MSC spans across a gap or pore in endothelial layer with portions remaining both apical and basal); and basal (stage 5). Two routes of transmigration (paracellular and transcellular) were defined as described [19] using the relative distribution of VE-Cadherin (an endothelial adherens junction marker), CD90 and VCAM-1. In paracellular transmigration, MSC migrated between two or more ECs with evident disruption of the VE-Cadherin stained adherens junctions (i.e., "paracellular gaps"). In transcellular transmigration, MSC migrated directly through an individual EC via a transcellular pore located at least 1 μm from an intact adherens junction. MSCs were scored as positive for membrane blebbing activity if at least one clear membrane bleb was present. Blebs were defined as hemispherical-shaped cell surface protrusions (seen through CD90 staining) of 1–5 μm in diameter. Filopodia were defined as thin spike or rod-like cell surface protrusions.

Fluorescence Plate Reader-Based Adhesion Assay

Adhesion assay was as previously described [25]. Briefly, confluent hCMVEC monolayers were grown in 96-well plates and, where indicated, preactivated with 50 ng/ml TNF-α for 16 hours. hMSCs were detached and incubated with a 0.5 μM solution of 2′,7′-bis-(2-carboxyethyl)-5-(and-6)-carboxyfluorescein (Molecular Probes, Eugene, OR, www.invitrogen.com) fluorescent dye for 15 minutes at room temperature in the dark in buffer A (Hanks' balanced saline solution [Invitrogen, Carlsbad, CA, www.invitrogen.com] supplemented with 20 mM HEPES [pH 7.2], 1% human serum albumin [HSA]). MSCs were washed once with buffer A and resuspended at 2×10^5 cells/ml in EBM-2MV. 50 μl of MSC suspension was added to each well of hCMVEC. In some cases, MSCs or EC were preincubated for 15 minutes with 20 μg/ml mouse anti-alpha 4 integrin or sheep-

anti-VCAM-1 function-blocking antibodies (or correlating species-matched IgG controls), respectively, prior to MSC-EC coincubation. Plates were subjected to a brief centrifugation (<10 seconds at 150 RCF) and then incubated at 37°C for 10 minutes. The fluorescence of each well was read on a SpectraMax M5 microplate reader (Molecular Devices, Sunnyvale, CA, www.moleculardevices.com) both immediately before and following two sequential washes with 100 μl of buffer A. Wells in which no MSCs were added were used to measure background fluorescence of the monolayer. Each condition was done in triplicate. Results are presented as the postwash fluorescence of each well divided by the prewash fluorescence.

Live-Cell Imaging of MSC on Endothelium

ECs and MSC were transfected by Amaxa electroporation according to the manufacturer's instructions (Lonza, Basel, CH, www.lonza.com) with the following constructs as indicated: green fluorescent protein (GFP)-actin (Clontech Laboratories, Mountain View, CA, www.clontech.com), palmitoylated yellow fluorescent protein (YFP) ("mem-YFP"; Clontech Mountain View, CA, www.clontech.com) and palmitoylated DsRed ("mem-DsRed;" Clontech [19]). For MSC nucleofection, 500,000 MSCs were resuspended in 100 μl of Amaxa hMSC Nucleofector solution. Next, 5 μg of the relevant plasmid (either mem-YFP or GFP-actin) was added to the MSC suspension and then the mixture was transferred to an electroporation cuvette, which was placed in the Amaxa electroporator and subject to the MSC-specific electroporation program U-23. MSC culture media (500 μl) was then added to the cuvette, the mixture was then transferred to a T75 flask containing 15 ml of MSC culture media. Transfected MSCs were incubated at 37°C/5% CO_2 for 24 hours before use. Survival rate was ~60% and transfection efficiency was ~50%. For hLMVEC nucleofection, 500,000 hLMVECs were resuspended in 100 μl of Amaxa hMVEC-L Nucleofector solution. Cells were then transfected as above using the endothelial-specific electroporation program S-005 followed by addition of EBM-2MV culture media and plating on Delta T culture dishes from Bioptechs (Butler, PA, www.bioptechs.com). Survival rate was ~50% and transfection efficiency was 40%–60%. Transfected ECs were used 48 hours after plating and 12–16 hours after activation with 50 ng/ml of TNF-α. Occasionally, ECs were alternatively stained with the fluorescent membrane marker Octadecyl Rhodamine B Chlorideme (R18; Invitrogen, Carlsbad, CA, www.invitrogen.com) immediately before live-cell imaging. R18 was mixed with PBS at a 1:2,000 ratio, and incubated with a confluent endothelial monolayer in the dark at 37°C for 10 minutes, followed by washing twice with EBM-2MV. Live-cell imaging was conducted on an Axiovert S200 epifluorescence microscope (Zeiss, Heidelberg, DE, www.zeiss.com) equipped with an Orca CCD camera (Hamamatsu, Shizuoka Pref., Japan, www.hamamatsu.com) and AxioVision software (Zeiss, Heidelberg, DE, www.zeiss.com), both ×40 and ×63 oil-immersion objectives and a Delta T heating stage (Bioptechs, Butler, PA, www.bioptechs.com) to maintain temperature at 37°C. At intervals of 5–90 seconds, sequential differential interference contrast (DIC), fluorescence, and interference reflection microscopy (IRM; a modality that explicitly reports regions of close cell-substrate interaction [26]) were acquired. Lateral migration velocities of apical MSC on endothelium (28 MSCs in four separate experiments) were obtained by tracking position of individual MSC over a 30-minute duration using the AxioVision Tracking Module.

Live-Cell Imaging of MSC on Fibronectin-Coated Glass

To quantify MSC blebbing in the presence or absence of adhesive signals, we performed live-cell imaging of MSC, with or without preincubation with the 120 kDa α-chymotryptic cell attachment region of fibronectin (Millipore, Billerica, MA, www.millipore.com), on fibronectin-coated glass. Delta T culture dishes from Bioptechs were incubated with a 40 μg/ml solution of human purified fibronectin (Invitrogen, Carlsbad, CA, www.invitrogen.com) for at least 1 hour. Approximately 100,000 MSCs were trypsinized and resuspended in 200 μl of buffer A, with or without 240 μg/ml of the cell attachment region of fibronectin. MSCs were incubated in suspension for 30 minutes at 37°C, pelleted, and then resuspended in 30 μl buffer A with 0.1% HSA (Sigma-Aldrich, St. Louis, MO, www.sigmaaldrich.com). 10 μl of the MSC suspension was then carefully transferred onto the fibronectin-coated Delta T dish containing 400 μl buffer A. At least 30 MSCs were then imaged in three random fields over three consecutive 6-minute durations. Live-cell imaging was conducted as above using a ×40 oil-immersion objective. Blebbing MSCs were then expressed as a percentage of the total number of MSC imaged.

Transmission Electron Microscopy

Transmission electron microscopy was performed as described previously [27]. Briefly, MSCs were incubated on TNF-α-activated GPNTs grown on fibronectin-coated glass for 30 minutes and then fixed with 2.5% glutaraldehyde and 2% paraformaldehyde in 1.0 M sodium cacodylate buffer, pH 7.4, for 2 hours, postfixed in 1.5% sym-collidine-buffered OsO_4 for 1 hour, stained en bloc with uranyl acetate, dehydrated in alcohol, and embedded in eponate. Thin eponate sections of 90 nm were visualized with a Philips CM-10 electron microscope.

Statistical Analysis

In our studies, we used pooled MSC donor data whereby an individual experiment (i.e., $n = 1$) was always done with MSC from a single donor and among the total averaged replicates at least two different donors were included. Results were presented as mean ± SEM for $n \geq 3$. For comparisons between two groups, Student's t tests were used. Comparisons between multiple groups (>2) were performed with one-way analysis of variance with Tukey's post hoc test, unless otherwise stated. Asterisks indicate statistically significant differences of $p < .05$ (*), $p < .01$ (**), or $p < .001$ (***).

RESULTS

MSC Transmigrate in an Inflammation-, Gαi-, and VCAM-1-Dependent Manner

To investigate the mechanisms for inflammation-specific extravasation of MSC, we set up in vitro models of "resting"/"quiescent" and cytokine-"activated" microvascular endothelium. Specifically, we cultured confluent monolayers of primary human lung (hLMVEC) and cardiac (hCMVEC) MVECs and activated them with the potent inflammatory cytokine TNF-α. MVEC activation was confirmed by strongly upregulated expression of the adhesion molecules VCAM-1 and ICAM-1 (supporting information Fig. S1A). Early passage (P3–P7) primary human bone marrow-derived MSCs (which were confirmed to be minimally senescent; supporting information Figure S1B [28]) were detached from tissue culture dishes and incubated on TNF-α-activated endothelial monolayers for 1 hour, followed by washing and fixation. Through imaging-based methods, we confirm previous observations [11, 12] that endothelial activation enhances MSC-endothelial interactions, as noted by increased density of MSC remaining associated with the endothelium (Fig. 1A).

To quantify and further characterize this observation, we used confocal fluorescence microscopy. This allowed for assessment of MSC positioning with respect to the endothelium in one of three states: (a) apical: completely on the upper/apical surface of the endothelial monolayer, (b)

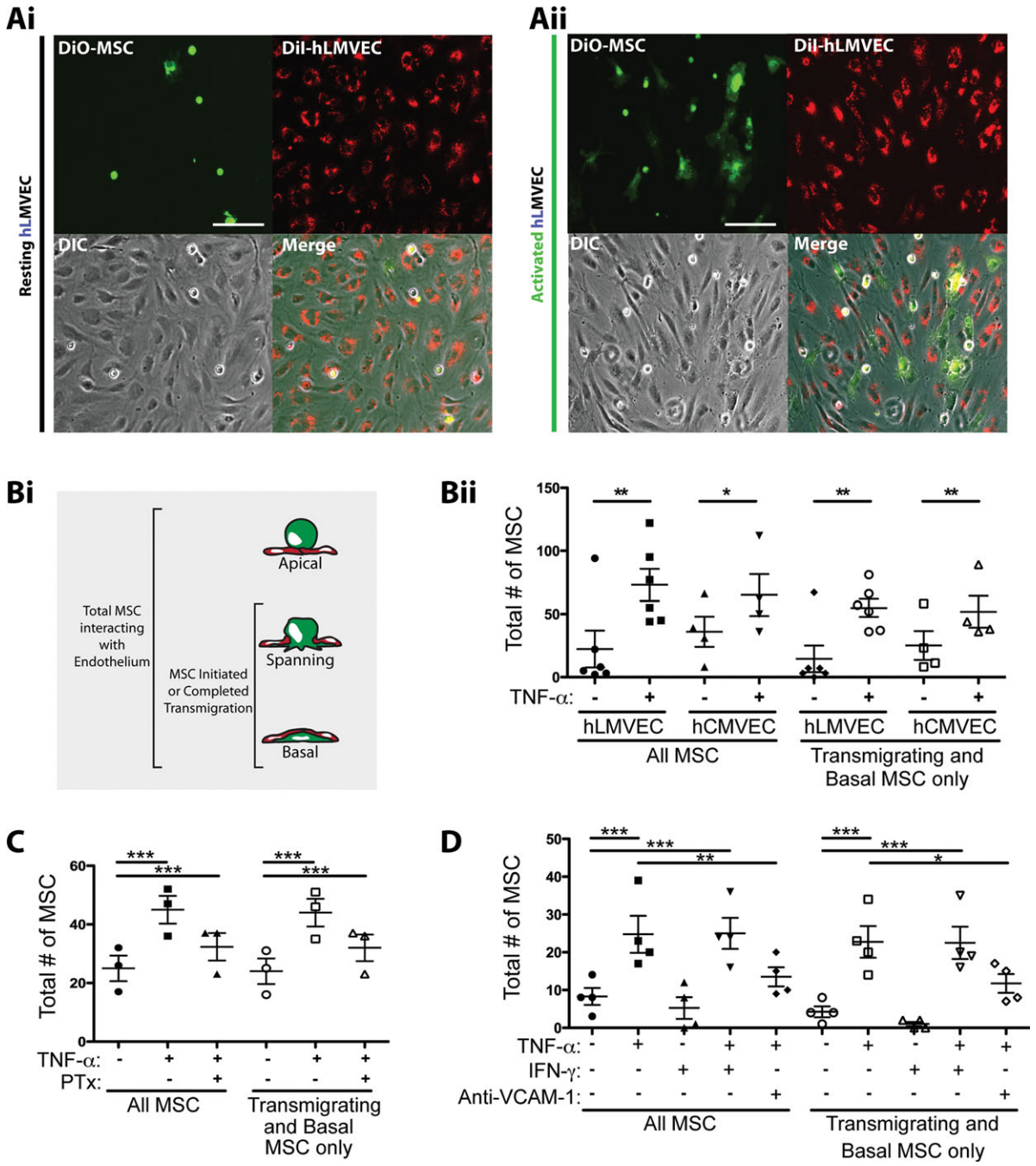

Figure 1. MSC preferentially transmigrate through TNF-α-activated lung and cardiac endothelium. (**A**): DiO-labeled MSCs (green) were incubated on resting (i) or TNF-α-activated (ii) DiI-labeled human lung microvascular endothelium (hLMVEC; red) for 60 minutes, followed by fixation and imaging by fluorescent and phase-contrast microscopy. Representative micrographs are shown. Scale bars represent 100 μm. (**B**): MSCs were incubated on resting or TNF-α-activated hLMVEC and hCMVEC for 60 minutes, followed by fixation, staining, and imaging by fluorescent confocal microscopy. (i) MSCs were counted and classified according to their positions relative to endothelium: apical, spanning, or basal. (ii) Both the total number of MSC and the number of MSC in only the transmigrating or basal positions were compared on TNF-α-activated and resting endothelium for both hLMVEC and hCMVEC. (**C**): MSCs were incubated on resting or TNF-α-activated hCMVEC for 60 minutes. In some cases, MSCs were incubated with 100 ng/ml of PTX for 2 hours prior to be added to endothelium. As in (B), both the total number of MSC and the number of MSC in only the transmigrating positions were compared for all conditions. (**D**): MSCs were incubated on resting, or TNF-α-activated and/or IFN-γ-activated hCMVEC for 60 minutes. In some cases, TNF-α-activated endothelium was incubated with 20 μg/ml blocking antibodies against VCAM-1 for 30 minutes prior to the addition of MSC. Samples were fixed, stained, and imaged by fluorescent confocal microscopy. As in (B), both the total number of MSC and the number of MSC in only the transmigrating or basal positions were compared for all conditions. For (Bii), (C), and (D), data were collected from at least six microscopic fields for each experimental condition. Values represent mean ± SEM. One, two, or three asterisks indicate three levels statistically significant differences ($p < .05$, $p < .01$, and $p < .0001$, respectively). For (B), this was assessed by a two-tailed, paired Student's *t* test. For (C) and (D), this was assessed by a one-way analysis of variance test with a Tukey post hoc test. Abbreviations: DIC, differential interference contrast; hCMVEC, human cardiac microvascular endothelial cell; hLMVEC, human lung microvascular endothelial cell; MSC, mesenchymal stem cell; PTX, pertussis toxin; TNF-α, tumor necrosis factor-alpha; VCAM, vascular cell adhesion molecule.

transmigrating: spanning across the endothelium and partially occupying both the apical and subendothelial/basal spaces, or (c) basal: completely under/basal to the endothelium (Fig. 1Bi, schematic). We interpreted these to represent MSC that had not yet initiated, were in the process of, or had completed transmigration, respectively. We quantified both total MSC (all three states; as a measure of overall interaction efficiency) as well as MSCs that were either transmigrating or basal to the endothelium (as a measure of transmigration frequency). In both cases, the numbers of MSC were increased 2–3-fold

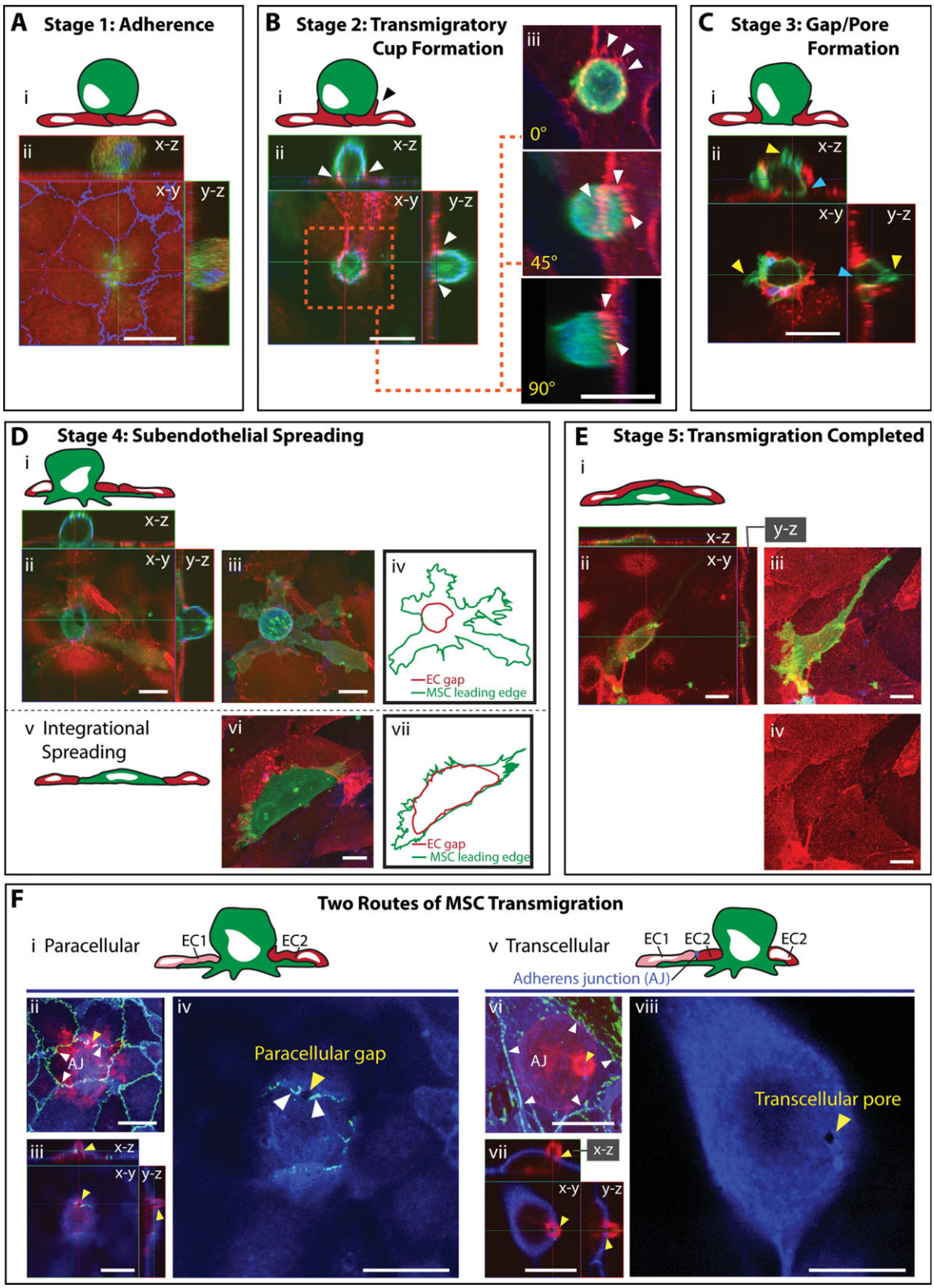

Figure 2. (legend on page 2478).

on TNF-α-treated endothelium (Fig. 1Bii) demonstrating that endothelial activation promotes both adhesion and transmigration of MSC.

Activated endothelia express and present a range of chemokines [8, 29] some of which have been implicated in MSC transmigration in bone marrow [30]. To probe the idea that MSC adhesion and transmigration in our model may be dependent in part on chemokines, we used PTX, a broad-acting inhibitor of chemokine receptor signaling via ADP-ribosylation of the G protein Gαi. Pretreatment of MSC with PTX (under conditions that did not alter cell viability; supporting information Fig. S2A), indeed significantly inhibited their adhesion to and transmigration across activated MVEC (Fig. 1C).

Previous studies have implicated the integrin very late antigen-4 (VLA-4) and its ligand VCAM-1 in MSC adherence to endothelium [11, 12]. We compared MSC adhesion and transmigration on TNF-α versus IFN-γ activated MVEC. Unlike TNF-α, IFN-γ was ineffective at upregulating VCAM-1 (supporting information Fig. S1A), and found that only TNF-α could promote MSC-MVEC interactions (Fig. 1D). Similar studies with a rat brain endothelial cell line (GPNT [21, 22]) in which both TNF-α and IFN-γ failed to significantly upregulate VCAM-1 (supporting information Fig. S1A) showed that both cytokines failed to upregulate MSC interactions (supporting information Fig. S2B). We found that function-blocking antibodies to VCAM-1 significantly blocked the TNF-α-mediated upregulation of MSC adhesion and transmigration on MVEC (Fig. 1D and supporting information Fig. S2C). Finally, function-blocking antibodies to the VCAM-1 receptor VLA-4 (which we confirmed was expressed by MSC; supporting information Fig. S2D) similarly block MSC-MVEC interactions (supporting information Fig. S2C).

MSC Actively Transmigrate Both Between and Directly Through ECs in Association with Transmigratory Cups

Previous studies with static imaging suggested that rather than transmigrating, MSC "integrate" into the endothelial monolayer by causing EC retraction and spreading on the underlying matrix [13–15]. This is in contrast to leukocytes that transmigrate through discrete pores and gaps in the endothelium and progressively spread underneath endothelium [19]. To determine whether MSCs integrate or actively transmigrate across the endothelium in our model of inflamed MVEC, we conducted detailed high-resolution confocal imaging analysis (Fig. 2). In samples fixed after 1 hour coincubation, we observed that some MSCs indeed underwent integration. However, we also largely encountered five distinct morphological arrangements consistent with progressive stages of a discrete and active transmigration process.

Stage 1—Adherence: relatively spherical MSC adhered to the flat apical surface of a continuous, intact endothelial monolayer (Fig. 2A). Stage 2—Transmigratory Cup Formation: adherent MSCs were partially "embraced" by microvilli-like endothelial projections that extended vertically and were enriched in actin and VCAM-1 (Fig. 2B, white arrows, and supporting information Video 1) in similar fashion to transmigratory cups formed during leukocyte diapedesis [19, 25, 31]. Contrasting leukocytes [8, 9], apically adherent MSC (i.e., stages 1 and 2) did not exhibit significant spreading or polarization. Stage 3—Gap/Pore Formation: transmigratory cup-associated MSC exhibited bulbous basal protrusions that extended across discrete gaps or pores in the endothelium, which were in direct contact with the underlying substrate (Fig. 2C, blue arrows). Stage 4—Subendothelial Spreading: MSC still remained partially above and spanning across the endothelium but showed increased amounts of membrane spread out beneath the endothelium (Fig. 2Di–2Div). Stage 5—Transmigration Completed: MSCs that had completed transmigration were spread entirely underneath the endothelial monolayer (Fig. 2E).

As noted above, varying fractions of MSC (~1% on GPNT, up to ~50% on hCMVEC) caused large-scale disruption of the endothelium, integrating into the monolayer rather than migrating across it (Fig. 2Dv–2Dvii). Using dynamic live-cell imaging, we further confirmed that MSC coincubation could lead to progressive retraction of endothelium coupled with MSC spreading on the substrate (data not shown). Although not quantified, we observed that integration events were more frequent when a given endothelial monolayer a priori exhibited relatively low confluence or showed signs or poor health and defective integrity (i.e., pre-existing

Figure 2. The five stages and two routes of MSC transmigration. Five distinct stages (**A**–**E**) of transmigration were consistently observed for MSC, based on previously established leukocyte morphological analysis [19], presented as both schematics (Ai; Bi; Ci; Di, iv, v, vii; Ei; Fi, v; see also supporting information Fig. S1) and confocal projections (Aii, Bii, iii, Cii, Dii, iii, vi; Eii–iv; Fii–iv, vi–viii). Confocal projections include top (*x*-*y*) and orthogonal (*x*-*z* and *y*-*z*) cross-sections. (A): Stage 1: Adherence. A relatively spherical MSC (CTx-B; green) is adherent to the apical surface of an intact GPNT monolayer as seen by ICAM-1(EC surface; red) and VE-cadherin (EC junctions; blue) staining. (B): Stage 2: Transmigratory Cup Formation. Vascular cell adhesion molecule-1 (VCAM-1)-enriched microvilli-like vertical projections (white arrows) that extend up from human lung microvascular endothelial cell (hLMVEC) endothelium (VCAM-1; red) and form a "cup-like" structure around the base of the MSC (CD90; green) at 60 minutes. Actin is stained in blue. Three-dimensional projections (rotated 0°, 45°, and 90° about *y* and *z* axes) are shown in (iii). See also supporting information Video 1. (C): Stage 3: Gap/Pore Formation. A discrete human cardiac microvascular endothelial cell endothelial discontinuity is occupied by the basal portion of an MSC in contact with the substrate (blue arrows) indicating initiation of transmigration at 60 minutes. Sample stained as in (B). Note blebs extending from the MSC surface (yellow arrows). (D): Stage 4: Subendothelial Spreading. A representative MSC is shown spreading beneath intact hLMVEC endothelium via a discrete gap. Orthogonal projections (ii) and a merged image (iii) are shown. This is in contrast to integration (schematic, v; orthogonal projection, vi), where MSC displace endothelial cells by spreading between adjacent EC. MSC leading edges and gaps in the EC are outlined in iv and vi to highlight the distinct endothelial gaps that are typically formed during transmigration through endothelium versus integration within an endothelial monolayer. Samples are stained as in (B). (E): Stage 5: Transmigration Completed. Representative orthogonal views (ii) indicate an MSC completely under the endothelium at 60 minutes. Top view projections, with (iii) or without (iv) MSC shown, demonstrating intact endothelium. (**F**): Two routes of MSC transmigration, paracellular and transcellular, are shown. MSC incubated on Gareth Pryce Newly Transformed (GPNT) rat ECs for 60 minutes were fixed and stained for VE-cadherin (green), CTx-B (MSC; red), and ICAM-1 (blue). Representative images of MSC at similar late stages in diapedesis migrating either through a paracellular gap between two endothelial cells (i–iv) or through a transcellular pore across a single endothelial cell (v–viii). Images are either top view projections of entire Z-stacks (ii and vi) or single sections alone (iv and viii) or together with orthogonal projections (iii and vii). The red MSC (CTx-B) signal was omitted for panels iv and viii to enhance visualization of the transmigration passageway. Note that in both events, only a small rounded portion of the MSC still remains above the endothelium. In ii–iv, the MSC migrates through a small (~2 μm in diameter) paracellular gap (iii, yellow arrows) between two cells where the adherens junction (AJ, white arrows) has been disrupted. In vi–viii, the MSC passes through a small (~1 μm in diameter) transcellular pore (vi, yellow arrow) distinct from intact adherens junctions (white arrows). Scale bars represent 20 μm. Abbreviation: MSC, mesenchymal stem cell.

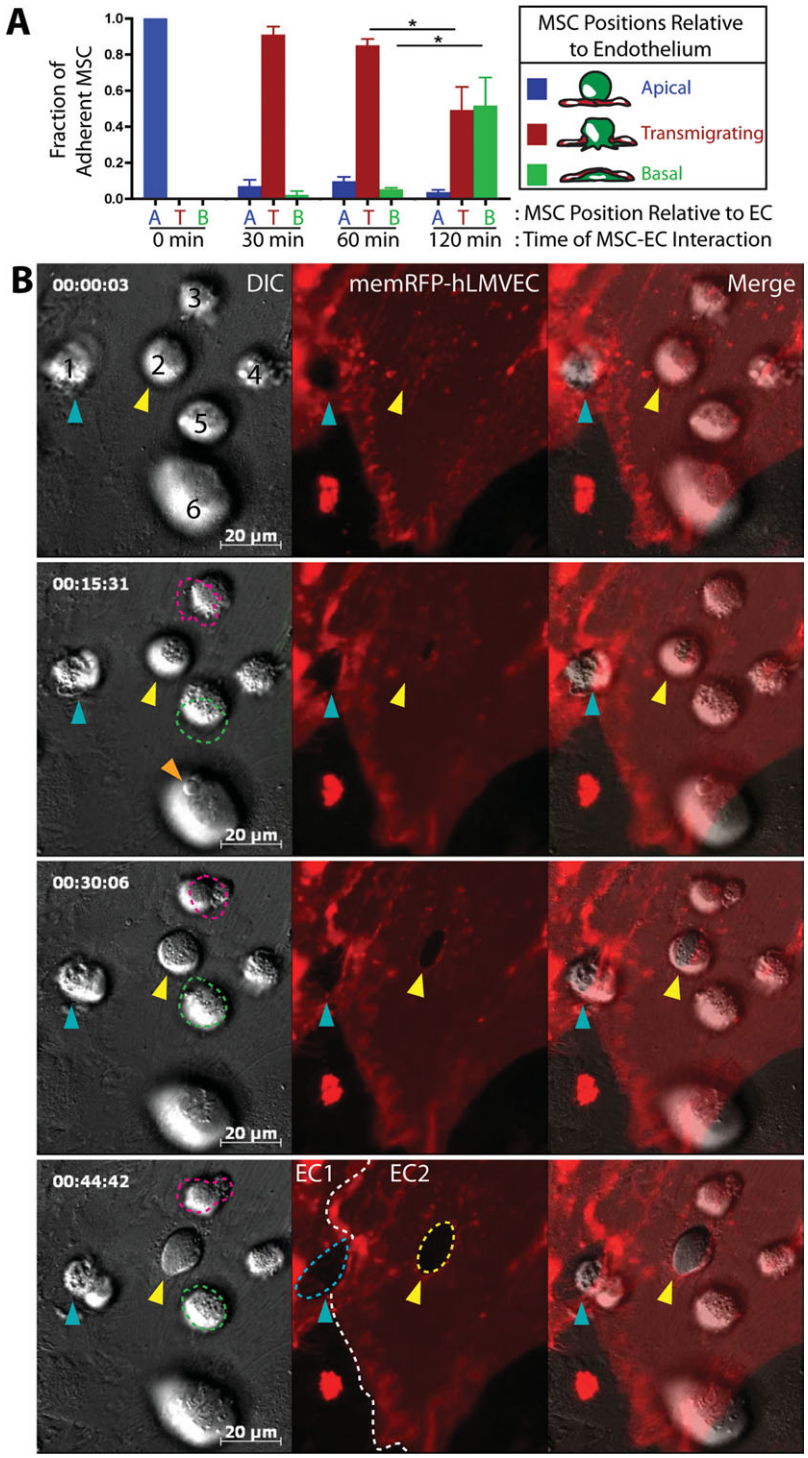

Figure 3. MSC transmigration kinetics and absence of lateral migration. (A): MSCs were incubated on hLMVEC for 30, 60, or 120 minutes, then fixed, stained, and imaged as in Figure 2. As in Figure 1B, MSCs were counted and classified according to their positions relative to endothelium: Apical, spanning, or basal. Values represent mean ± SEM. Asterisks indicate a statistically significant difference ($p < .05$) as assessed by a one-way analysis of variance test with a Tukey post hoc test, $n = 3$. (B): MSCs were subjected to live-cell DIC (left panels) and fluorescence (middle panels) imaging during interaction with activated memDsRed-transfected hLMVEC (red). Still frames from the video at 0, 15, 30, and 45 minutes are shown. Numbers identify six separate MSC. Blue and yellow arrows indicate two MSC (#1 and #2) in the active process of transmigration as indicated in part by the expanding transmigration passage ways in the endothelium; white dashed lines (middle panels, bottom row) indicate intercellular junctions between two ECs ("EC1" and "EC2"), blue dashed line indicates a paracellular gap for migration of MSC #1, and yellow dashed line indicates a transcellular pore for transmigration of MSC #2. Pink and green dashed lines (left frames; MSC #3 and #5) represent the location of two different apical MSC in the preceding panel (i.e., lines at 15 minutes panel show the MSC positions in 0-minute panel, etc.) and highlight a lack of significant lateral migration. Orange arrow, MSC #6 (15 minutes time point) indicates the protrusion of an MSC bleb against the endothelial surface. See also supporting information Video 2. Scale bars represent 20 μm. Abbreviations: DIC, differential interference contrast; hLMVEC, human lung microvascular endothelial cell; MSC, mesenchymal stem cell.

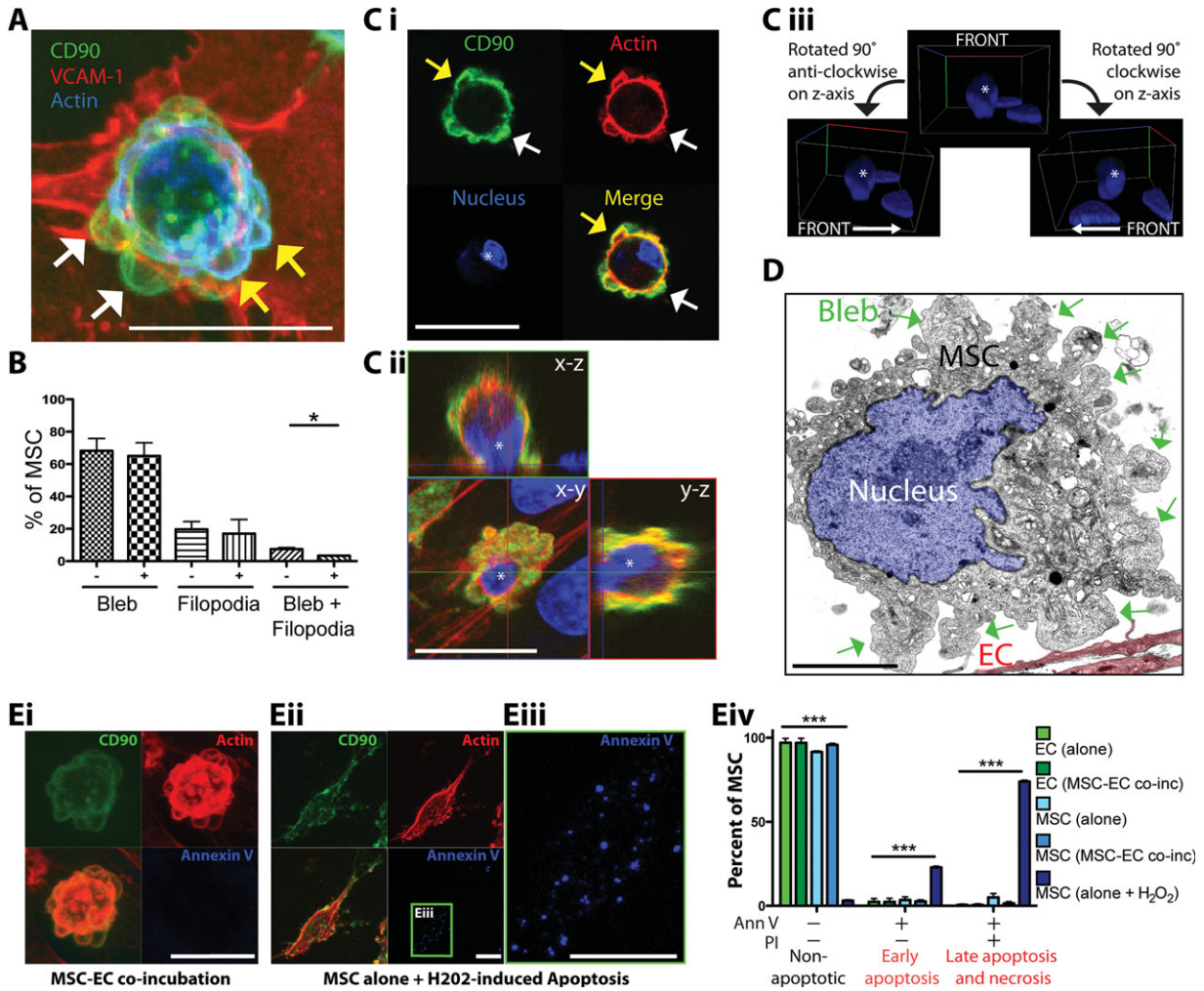

Figure 4. MSCs exhibit extensive nonapoptotic blebbing on endothelium. (A): MSCs were incubated for 60 minutes on activated human lung microvascular endothelial cell (hLMVEC), then fixed and stained for CD90 (green), vascular cell adhesion molecule-1 (red), and actin (blue). A representative top view confocal projection of a MSC at an early-stage of transcellular diapedesis is shown. Multiple highly rounded, bleb-like structures can be seen protruding from the MSC surface, which are both negative (white arrows) and positive (yellow arrows) for cortical F-actin (blue). See also supporting information Video 3. (B): MSCs were incubated on resting or TNF-α-activated human cardiac microvascular endothelial cell for 60 minutes. At least 30 MSCs were counted for each condition per experiment ($n = 3$). The fraction of MSC exhibiting either blebs, filopodia, or both was quantified as shown. Values represent mean ± SEM, $p < .05$, as assessed by paired Student's t test. See also related supporting information Video 4. (C): MSCs were incubated for 60 minutes on activated hLMVEC and then fixed. To ascertain whether or not blebbing reflected MSC apoptosis, samples stained for CD90 (green), actin (red), and nuclear morphology (ToPro3; blue). A representative example of early-stage diapedesis is shown. Both single top view (x-y plane) confocal sections (i) and top view projections/orthogonal cross-sections (ii) clearly presents F-actin negative (white arrows) and positive (yellow arrows) and blebs over all MSC surfaces, including those in direct contact with the endothelium. The MSC nucleus (distinguished from neighboring endothelial nuclei with an asterisk) shows normal intact morphology (rather than the canonical fragmented morphology seen during apoptosis) as seen by confocal cross-section (i), orthogonal view (ii), and three-dimensional volumetric rendering (iii). (D): MSCs were incubated for 30 minutes on Gareth Pryce Newly Transformed (GPNT) rat ECs, fixed and then processed for, and imaged by transmission electron microscopy. Micrograph depicts a representative MSC on endothelium (EC, 10% opacity red overlay) with clearly evident micron-scale cell surface blebs (green arrows) and an intact nucleus (highlighted with a 10% opacity blue overlay). (E): (i–iii) MSCs were either incubated on hLMVEC for 30 minutes or on tissue culture plastic in the presence of 5 mM hydrogen peroxide for 2 hours, followed by fixation and staining for CD90 (green), F-actin (red), and annexin V (blue). Representative images show confocal projections of annexin V-negative blebbing MSC on hLMVEC (i) and annexin V-positive MSC exhibiting hydrogen peroxide-induced apoptosis (ii and iii). (iv) Flow cytometric analysis of annexin V- and propidium iodide (PI)-stained EC (shades of green) and MSC (shades of blue) following separate culture (with or without 2 hours treatment with 5 mM hydrogen peroxide for MSC) or 1 hour EC-MSC coincubation. Percentage of cells in each condition that were nonapoptotic (annexin V and PI negative), in early apoptosis (annexin V positive, PI negative) and late apoptosis/necrosis (annexin V and PI positive) are shown. Values are mean ± SEM, $n = 3$. Asterisks indicate a statistically significant difference as assessed by a one-way analysis of variance test with a Tukey post hoc test. Scale bars represent 20 μm for (A), (C), and (E) and 5 μm for (D). Abbreviations: MSC, mesenchymal stem cell; VCAM, vascular cell adhesion molecule.

intercellular gaps). On our blood-brain-barrier endothelial model (i.e., GPNT), which consistently provided an endothelial barrier of exceptionally high integrity, MSC integration was only very rarely observed and transmigration nearly always occurred through highly discrete gaps and pores (e.g., Fig. 2F).

Significantly, in the course of the above investigation, we noted that apart from integration, MSC apparently could use

two distinct pathways or "routes" for crossing the endothelial barrier like leukocytes [10]. In the majority of diapedesis events, the MSC migrated across paracellular gaps via the local disruption of the adherens (supporting information Fig. S3A) and tight (supporting information Fig. S3B) junctions. Interestingly, JAM-1 (a tight junction marker [32]) also exhibited modest enrichment in transmigratory cups (supporting information Fig. S3C). Less frequently (~20%–30% of diapedesis events) MSC migrated directly through individual ECs via de novo formation of transcellular pores in ECs (Fig. 2Fv–2Fviii).

MSC Undergo Relatively Slow Transmigration in the Absence of Lateral Migration

Next, to assess the kinetics of MSC transmigration, we incubated the MSC with the activated hLMVEC for 30, 60, and 120 minutes and then quantified the fraction of MSC that were apical, transmigrating, or basal to endothelium as in Figure 1. These studies showed that >90% of adherent MSC initiated transmigration within 30 minutes, while approximately 50% completed the process only after 120 minutes (Fig. 3A).

To better integrate the stages of transmigration observed through fixed-cell studies (i.e., Fig. 2), we turned to live-cell microscopy. Consistent with the fixed-cell imaging studies, adherent MSC (i.e., that had not yet transitioned to gap/pore formation) retained a relatively spherical morphology. MSC also exhibited very limited net lateral movement over the endothelial surface; although movement velocities averaged 3.08 ± 0.3 μm/minute, total displacement over 30–60 minutes was usually only ~1–3 μm (Fig. 3B and supporting information Video 2, MSC #3–6). Additionally, live-cell imaging revealed that the formal phase of transmigration (i.e., initial formation of a gap or pore until the completion of diapedesis) is a relatively slow process. Whether migrating paracellularly or transcellularly, MSC typically required at least 45 minutes

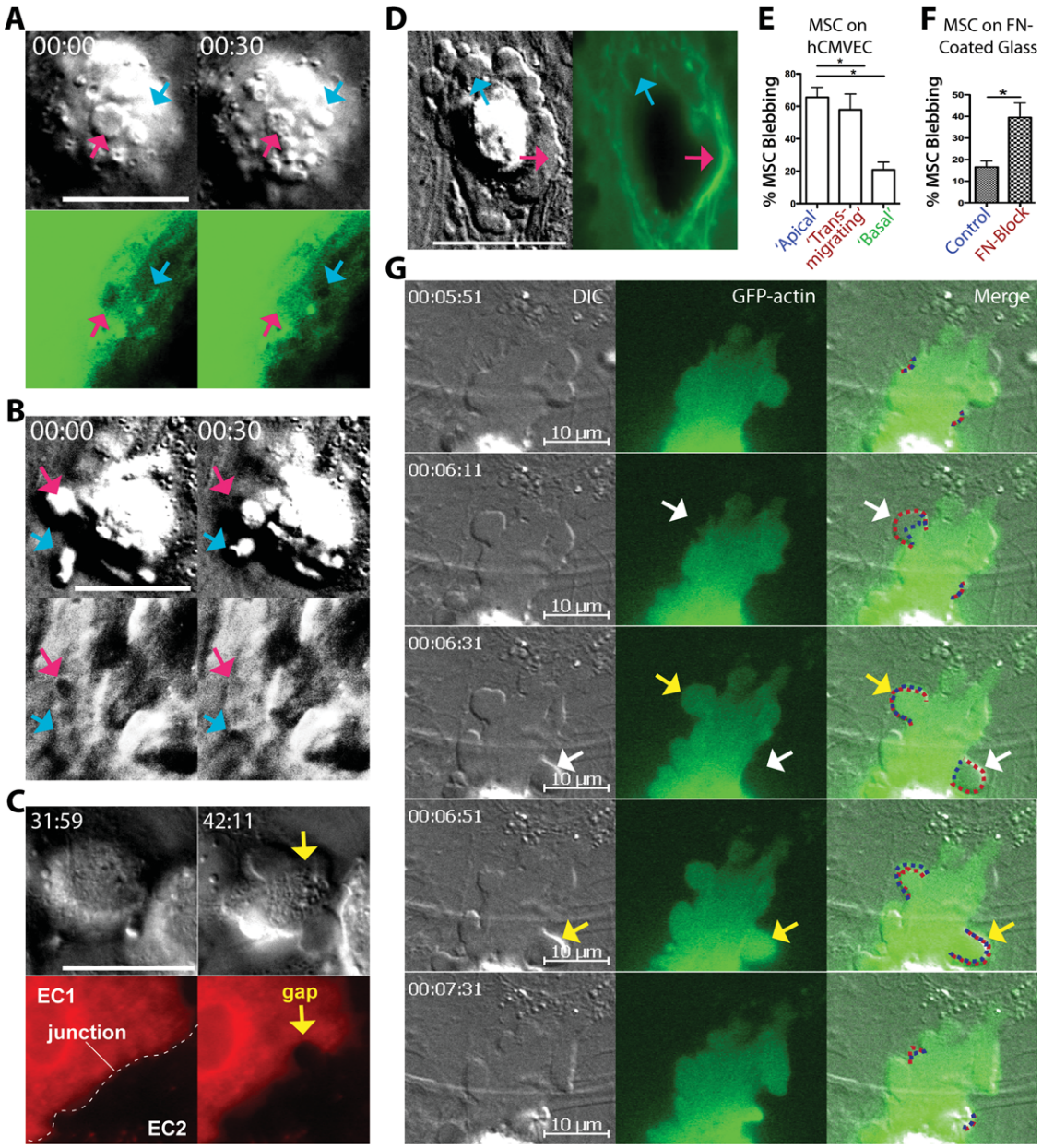

Figure 5. (legend on page 2482).

for this phase of migration (Fig. 3B and supporting information Video 2, MSC #1 and #2). It should be noted, however, that such extended durations precluded the visualization of complete transmigration events (i.e., stages 1–5) for individual MSC, due to technical challenges associated with such long-term imaging (e.g., cytotoxicity and photobleaching).

Transmigrating MSCs Exhibit Extensive Nonapoptotic Membrane Blebbing

The above findings (Figs. 2, 3 and supporting information Video 2) show an absence of polarization, limited lateral migration, and lack of characteristic protrusive structures (e.g., lamellipodia, pseudopodia and invadosomes [8, 9]) associated with leukocyte diapedesis. However, these initial live-cell imaging studies showed instead dynamic extension and retraction of membrane bleb-like protrusions (e.g., supporting information Video 2, MSC #5 and #6), and apparently related, more amorphous "worm-like" protrusions with somewhat longer lifetimes (e.g., supporting information Video 2, MSC #3 and #4). We had also noted apparent "snap-shots" of such protrusive activity in initial fixed-cell imaging (e.g., Fig. 2C, yellow arrows).

Further high-resolution imaging of this phenomenon clearly showed that blebs were formed over all surfaces of the MSC, including those in intimate contact with endothelium and at sites of endothelial pore or gap formation (Fig. 4A and supporting information Video 3). Interestingly, we observed that classic F-actin-free cell surface membrane blebs (in which the membrane had apparently detached from the underlying cortical actin layer; Fig. 4A, 4C, white arrows, and supporting information Video 3) coexisted in individual MSC with morphologically similar blebs that were strongly enriched in F-actin at the outer membrane (Fig. 4A, 4C, yellow arrows, and supporting information Video 3). Qualitative (supporting information Video 4) and quantitative (Fig. 4B) analysis revealed that the majority of MSCs, whether on resting or activated endothelium, exhibited blebs, whereas a minority exhibited filopodia instead. It is unknown whether filopodia-possessing MSCs are a distinct subset from blebbing MSC; however, a small subset of MSC expressed both filopodia and blebs (Fig. 4B), indicating that filopodia and blebs were not necessarily mutually exclusive.

Blebbing is classically associated with apoptosis. However, some embryonic and tumor cells have been shown to use nonapoptotic migratory blebbing for motility and invasion [16–18]. To determine whether or not blebbing MSCs were undergoing apoptosis, we stained the nuclei with ToPro3 and conducted high-resolution confocal imaging and digital 3D-reconstruction. In all cases, nuclei of blebbing MSC were healthy and intact, showing none of the canonical nuclear fragmentation that is associated with apoptosis (Fig. 4C, see asterisks in i-iii). This observation was confirmed by transmission electron microscopy imaging of nuclei (Fig. 4D). Furthermore, MSC cultured alone or coincubated with EC showed a lack of detectable staining for Annexin V or PI, as

Figure 5. MSCs use nonapoptotic blebs to exert force on surroundings. (A): MSCs were imaged live on TNF-α-activated hCMVEC transfected with soluble GFP (sGFP). We previously established that sGFP serves as a sensitive readout for local cytoplasmic volume and, indirectly, surface topology of endothelial cells [27]. Images show sequential still frames of a single MSC on an sGFP-expressing hCMVEC at 30-second intervals. By DIC, blebs can be seen protruding from the basal surface of the MSC against the endothelial cell surface (arrows). Note that at $t = 0$-second one bleb (pink arrow) has formed that corresponds to a decrease in local sGFP signal indicating an endothelial cell surface depression/invagination and consequent displacement of cytoplasm. In the subsequent frame that bleb has partially retracted and the endothelial depression has disappeared. At the same time, a distinct bleb and endothelial depression (blue arrow) form de novo. (B): MSCs were imaged live on TNF-α-activated hCMVEC with both DIC (top row) and interference reflection (bottom row; interference reflection microscopy [IRM]) microscopy. Images are sequential still frames of a single MSC on hCMVEC at 30-second intervals. At $t = 0$-second, one bleb (pink arrow) has generated a dark area in the corresponding IRM image indicating that the basal surface of the endothelial cell has been locally depressed and forced into close opposition with the underlying glass substrate. In the subsequent frame, this bleb retracts and the endothelial depression (i.e., IRM dark spot) disappears. At the same time, a distinct bleb and endothelial cell depression (blue arrow) form de novo. See also similar experiment in supporting information Video 5 "Example 2." (C): MSCs were imaged live on TNF-α-activated, mem-RFP transfected human lung microvascular endothelial cell (hLMVEC) with both DIC (top row) and fluorescence (bottom row) microscopy. Images are still frames separated by a ~10 minutes interval. Left panels show an MSC adherent over an intact intercellular junction (dashed line) formed between a positive mem-RFP transfected (EC1, red) and a nontransfected (EC2, black) hLMVEC. Right panels show that commensurate with the onset of blebbing, a large (~5 μm) rounded intercellular gap forms under the MSC. See also corresponding supporting information Video 5, "Example 4." (D): MSCs were imaged live on mem-GFP transfected hLMVEC with both DIC (left) and fluorescence (right) microscopy. Images are still frames of a single MSC migrating through a transcellular pore in a mem-GFP-positive endothelial cell. For this "fried egg-shaped" MSC, the peripheral blebbing regions of the MSC have already spread beneath the endothelium (supporting information Fig. S1, bottom, right "multiple leading fronts"), where the central "yolk" region is spanning across and partially above the endothelium. Arrows indicate dynamic MSC blebs expanding and apparently exerting force on the endothelium as seen by corresponding distortions in the endothelial cell topology. See the corresponding dynamics in supporting information Video 5, "Example 5." (E): The extent to which "non-apoptotic migratory blebbing" was associated with MSC at different stages of transmigration was quantified. MSCs were incubated on TNF-α-activated hCMVEC for 30, 60, or 120 minutes. Individual MSCs were classified according to their position (as in Fig. 1B) relative to endothelium and the percentage of blebbing MSC in each position is shown. Five independent experiments were performed, and a total of 85, 133, and 45 apical, transmigrating, and basal MSC, respectively, were counted. Values represent mean ± SEM. $*p < .05$, as assessed by unpaired Student's t test. (F): The association between MSC blebbing and avidity for a rigid substrate was explored. MSCs were incubated in either serum-free media ("Control"), or serum-free media containing 240 μg/ml of the α-chymotryptic fragment (cell attachment region) of fibronectin ("FN-Block") for 30 minutes, before being transferred to a fibronectin-coated glass dish. Three consecutive 6-minute videos of MSC were captured for each experimental condition, and the percentage of MSC which exhibited blebbing (described in Materials and Methods) is shown. Values represent mean ± SEM. $*p < .05$, as assessed by paired Student's t test. (G): GFP-actin (green; central and right panels)-transfected MSCs were imaged live during transmigration across activated hLMVEC via both DIC and fluorescence microscopy. The depicted example shows a relatively late stage diapedesis event (i.e., slightly advanced stage compared to Fig. 5D) in which the MSC is advancing part of its membrane under the endothelium through cycles of bleb expansion and retraction. Images are sequential still frames at 20- or 40-second intervals. Consistent with the fixed-cell imaging in Figure 4A and 4C, blebs can be seen (via the DIC imaging; left and right panels) protruding from the MSC that are both negative (white arrows) and positive (yellow arrows) for GFP-actin. Red dashed lines (right panels) delineate the edge of MSC membrane during bleb formation, whereas blue dashed line indicates the "edge" GFP-actin signal. Note that cycles of actin-negative bleb formation, followed by actin recruitment to the bleb and subsequent bleb retraction occur as the cell advances, features are highly similar to nonapoptotic migratory blebbing activities exhibited by some tumor and embryonic cell types [16–18, 33]. See also supporting information Video 7. Scale bars represent 20 μm. Abbreviations: DIC, differential interference contrast; GFP, green fluorescent protein; hCMVEC, human cardiac microvascular endothelial cell; MSC, mesenchymal stem cell.

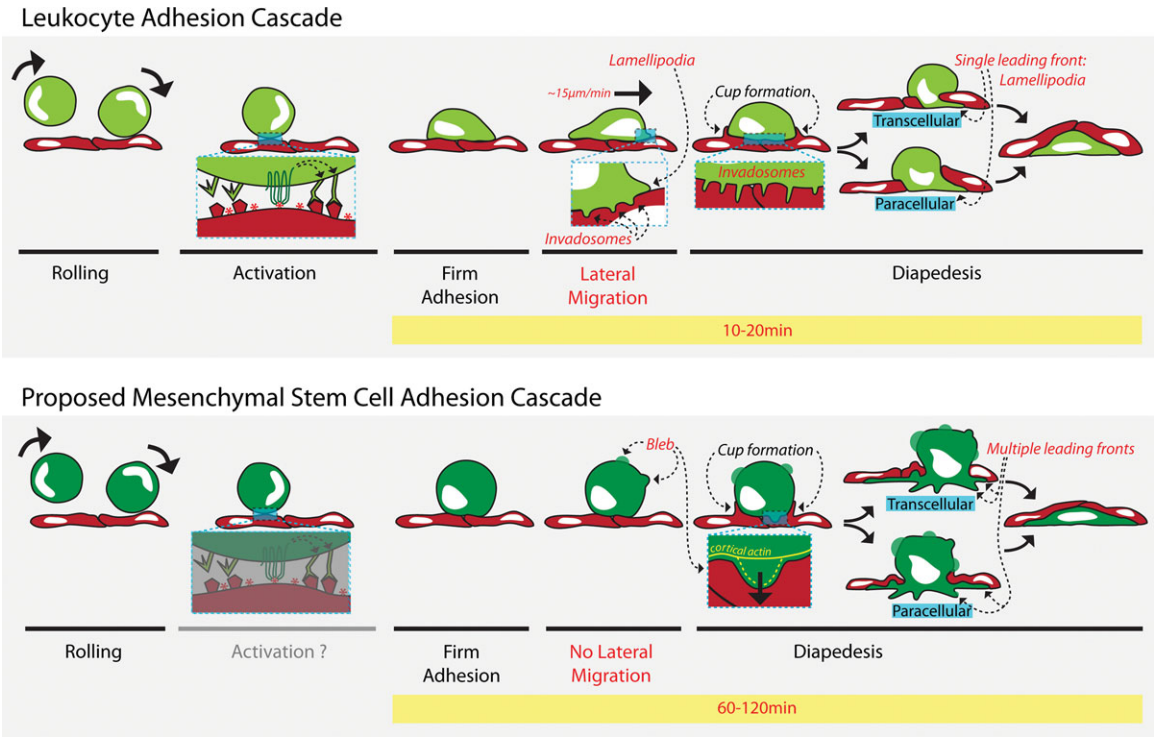

Figure 6. Comparison between the leukocyte transmigration cascade and the proposed mesenchymal stem cell (MSC) transmigration cascade. Discrete steps in the leukocyte adhesion cascade (top panel) and the proposed MSC adhesion cascade (bottom panel). Labels in red indicate key differences between the two processes, while labels in black indicate similarities. Leukocytes (light green) roll on activated endothelium (red) via selectins, which are upregulated on the endothelial surface during inflammation. MSC (dark green) also roll on endothelium [11]. Rolling brings leukocytes in proximity to the endothelial surface where chemokines (red asterisks) are presented. G-protein-coupled receptors on the leukocyte (top left inset) recognize the chemokines, leading to conformational rearrangements of leukocyte surface integrins adhesion receptors that are coupled to increased ligand binding affinity. This allows high affinity binding to complementary ligands such as ICAM-1 and vascular cell adhesion molecule-1 (VCAM-1) on the endothelial cell surface endothelial surface thereby inducing firm adhesion of the leukocyte. Although firm adhesion of MSC occurs [11], it is currently unknown whether this occurs through a similar activation step (bottom left inset). For leukocytes, adhesion is followed by an important phase of polarization and lateral migration, during which they use actin-dependent protrusions, including lamellipodia, pseudopodia, and invadosomes, for motility (top middle inset) and migratory pathfinding (top middle and right inset). In contrast, MSCs do not exhibit significant polarization or lateral migration on the apical surface of the endothelium. Moreover, there is no evidence that MSCs use lamellipodia, pseudopodia, or invadosomes during initiation of diapedesis. Intriguingly, however, they do display distinct and highly dynamics nonapoptotic blebbing protrusions. These form initially without cortical actin (bottom right inset, yellow line) but subsequently become enriched in actin (dashed yellow line), which is followed by bleb retraction. In some tumor and embryonic cell types such nonapoptotic blebbing serves as mechanistic basis for motility and invasion [16–18, 33]. Blebs are proposed here as putative mechanisms by which MSCs exert force on the endothelial surface (bottom right inset, black arrow), or search for adhesion points and sites permissive for transmigration. Although they appear to initiate transmigration through different protrusive activities, leukocytes and MSC both trigger proactive endothelial extension of microvilli-like, actin, ICAM-1, and VCAM-1 endothelial projections that form transmigratory cups, which are thought to facilitate diapedesis. Additionally, both cell types exhibit the ability to use transcellular (directly through an endothelial cell) and paracellular (between endothelial cells) routes of transmigration. However, leukocytes invade the subendothelial space typically with a single lamellipodial leading edge and complete the entire transmigration process in several minutes, while MSC initially spread beneath the endothelium in a starburst fashion with multiple leading fronts and require 1–2 hours to completely transmigrate.

assessed by microscopic (Fig. 4Ei–4Eiii) and flow cytometric analyses (Fig. 4Eiv).

MSC Display Nonapoptotic Blebbing in Association with Early Transmigration Stages and Can Exert Forces on Endothelium

To elucidate the dynamics of MSC blebbing during transmigration, we conducted live-cell imaging on TNF-α-activated endothelium. High temporal resolution DIC imaging revealed repetitive cycles of rapid bleb expansion (average time of 15.22 ± 0.92 seconds to reach maximal size of 1–5 μm), followed by a significantly slower phase of retraction (average time of 43.52 ± 2.40 seconds) (supporting information Video 4, "Example 1"). These kinetics are highly consistent with those of migratory blebs formed by some tumor and embryonic cells [16–18].

As noted with the fixed-cell imaging studies, blebs protruded from all surfaces of the MSC including those in direct contact with the endothelium. Blebs that formed against the endothelium often were coupled with "jerky" MSC movements suggesting that significant intercellular forces were being developed (e.g., supporting information Video 2, MSC #3, #4, and #6 [note orange arrow] and supporting information Video 5, Examples 2–4). Next, we conducted studies using EC transfected with soluble GFP, previously developed to monitor local cytoplasmic volume in EC as a readout for topological dynamics [27]. We found that as MSC protruded blebs against endothelium, spatially and temporally correlated regions of low GFP intensity were developed in the apposing EC (Fig. 5A). We interpreted this to signify formation of cytoplasm-displacing endothelial invaginations caused by MSC blebs driving the apical surface of the endothelium toward its basal surface. We confirmed this interpretation with

IRM, a modality that reveals regions of close cell-substrate apposition as dark areas [26] (Fig. 5B and supporting information Video 5, Example 2).

Further studies, in which ECs were transfected with plasma membrane markers (i.e., mem-DsRed or mem-YFP), suggest that blebs continue to form and exert forces during endothelial gap/pore formation (Fig. 5C and supporting information Video 5, Examples 3 and 4) and subendothelial spreading (Fig. 5D and supporting information Video 5, Example 5). Toward the end of the transmigration process, when MSC had formed significant contacts with the subendothelial fibronectin, blebbing was progressively diminished and replaced by radially spreading lamellipodia (supporting information Video 5, Example 5). Quantitative fixed-cell analysis confirmed that the majority of apical or transmigrating MSCs were associated with nonapoptotic migratory blebs, whereas those that were basal to endothelium had largely lost their blebs (Fig. 5E).

Nonapoptotic migratory blebbing in general has been suggested to reflect a cell's response to reduced substratum adhesion [16, 17, 34]. We hypothesized that modestly avid adhesion of MSC to endothelium may be permissive for blebbing, whereas high avidity adhesion to subendothelial matrix is not. To test this idea, MSCs in suspension were preincubated with or without the soluble cell-binding fragment of fibronectin and then seeded on fibronectin-coated substrate. As expected, control MSC exhibited very limited blebbing and initiated lamellipodial spreading almost immediately (Fig. 5F and supporting information Video 6, Part 1). However, when adhesion to the fibronectin-coated substrate was blocked, spreading was blocked (not shown) and MSC blebbing was preserved (Fig. 5F). Interestingly, when fibroblasts were seeded on activated endothelium, no blebbing was observed demonstrating that the blebbing response is not universal (supporting information Video 6, Part 2).

Finally, we performed live-cell imaging of MSC transfected with GFP-actin. These studies show that individual MSC blebs formed during transendothelial migration consistently exhibited cycles of rapid protrusion of actin-free blebs, followed shortly by recruitment of actin to the bleb and finally a somewhat slower phase of bleb retraction (Fig. 5G and supporting information Video 7). This was in agreement with our high-resolution confocal imaging that showed coexistence of both cortical actin-free and F-actin-enriched MSC blebs (Fig. 4A, 4C, white and yellow arrows, and supporting information Video 3). Importantly, as seen Figure 5G and supporting information Video 7, these cycles were coupled to the advancement of the subendothelial leading edge of the transmigrating MSC. Overall, these features are highly consistent with migratory blebbing mechanisms previously characterized in other cells [16, 17].

Discussion

Exogenously infused and endogenous MSCs are known to circulate and preferentially engraft at sites of inflammation in vivo. However, the process by which they migrate across the endothelial barrier to exit the circulation and engraft has remained incompletely understood. Here, we uncover a transmigratory process that combines leukocyte-like and unique mechanistic features (Fig. 6).

The molecular mechanisms underpinning the specificity of MSC extravasation at sites of inflammation likely includes activation of endothelium by proinflammatory cytokines. TNF-α stimulates expression and presentation of a range of chemokines and adhesion molecules by ECs [8, 29]. Consistent with previous reports [12, 14, 35, 36], we observed that both MSC adhesion and transmigration increased upon activation of endothelium with TNF-α. This in turn was mediated through Gαi (and thus likely chemokine)- and VLA-4/VCAM-1-dependent mechanisms. With respect to chemokines, two recent studies have directly implicated roles for CXCL9, CXCL16, CCL20, and CCL25 (for which MSC express cognate receptors) in augmenting transmigration [30, 35]. It is likely that other surface proteins and soluble factors, such as matrix metalloproteases [37, 38], are also involved that remain to be further investigated.

The cellular basis for MSC transmigration has been much less well-resolved. Previous reports that attempted to morphologically characterize the process of MSC transmigration, albeit with limited resolution, have described a process termed integration [13–15]. In such studies, large-scale retraction of endothelium coupled to MSC spreading on the substrate was inferred from static images. In this study, we aimed to improve upon the current knowledge using both high-resolution and dynamic imaging modalities in combination with specific molecular markers. In this way, we confirm that MSC coincubation can induce progressive retraction of large regions of endothelium that accommodate MSC spreading and integration. In addition, we also demonstrated for the first time that MSC can also mediate two other types of transmigration, namely, paracellular and transcellular diapedesis. Contrasting integration, the endothelium remained largely intact during diapedesis and MSC actively squeezed through discrete pores and gaps in the endothelium to enter the subendothelial space. The finding that MSC can initiate transcellular diapedesis is particularly compelling evidence that MSC can actively breach endothelial barriers as, contrasting paracellular gaps, transcellular endothelial pores never form autonomously in these settings [19, 27].

We also noticed that during diapedesis, the endothelium projected actin-, VCAM-1-, and JAM-1-rich finger-like protrusions from its surface that surrounds the MSC forming transmigratory cups similar to those shown to guide leukocyte transmigration [19]. This suggests that MSC diapedesis is also a cooperative event between both MSC and ECs. Whether JAM-1 localization to transmigratory cups is a result of engagement of a specific ligand on MSC or occurs through some type of lateral association with VCAM-1 [39] remains an open question.

While technical improvements in imaging may partly account for why diapedesis was observed for the first time in this study, it is also likely that the quality of endothelial monolayers used affects the fraction of diapedesis versus integration events observed. Although endothelial monolayers cultured in vitro are generally regarded to be an acceptable model for endothelium, many aspects of physiologic endothelium that promote junctional stability are absent or aberrant in vitro [40]. For example, endothelium is usually plated on nonphysiologically rigid substrates in vitro, which inclines them toward a hypercontractile phenotype [41] that is prone to intercellular gap formation and retraction [42, 43]. Other physiologic barrier-promoting or "anti-contractility" stimuli, such as steady-state laminar fluid shear flow, contacts with mural cells (e.g., pericytes), and exposure to circulating sphingosine-1 phosphate are also absent in most in vitro models. Thus, in vitro endothelia seem significantly biased toward less stable and more contractile phenotypes that may favor integration over to diapedesis. Consistent with this, we found that when poor/unhealthy EC monolayers were used MSC integration increased, whereas well-formed healthy monolayers exhibited less integration. Our in vitro EC model that retained the most physiologic and robust barrier properties (i.e., GPNT) allowed for almost negligible MSC integration. Thus, whereas we cannot rule out a role for integration as a physiologic mode of extravasation (as shown for some metastatic tumor cells [44, 45]), our observations suggest that it may often be overestimated in in vitro.

An important contrast between MSC and leukocyte diapedesis is that it occurred over a much longer time frame (30–120 vs. 3–6 minutes [19]) and in the absence of significant polarization, directed lateral migration and formation of lamellipodia or invadosomes. Our studies were performed under static conditions. A recent study showed that application of physiologic shear flow promoted slow lateral migration on the endothelium ($\sim$20 μm over $\sim$2 hours), although the MSC similarly failed to spread or polarize and required similar durations before spreading on the subendothelial matrix [35].

Unexpectedly, we found that MSCs display extensive nonapoptotic membrane blebbing during transmigration (Fig. 6). Nonapoptotic blebbing is a recently appreciated behavior used by some embryonic and tumor cells for motility and invasion [16–18]. We showed that dynamic features of MSC blebbing were similar to those described for other cells. Such blebbing has been shown to be a response of cells to a loss of substrate adhesion [16, 17, 34]. We noted that MSC blebbing was predominant in early stages of transmigration, in which MSCs were primarily contacting endothelium and rounded, but was lost at late stages of when MSC mediated extensive adhesions with and spread on the subendothelial matrix. Our data support the hypothesis that relatively low avidity interaction between endothelium and MSC is permissive for MSC blebbing, whereas the high avidity interactions that form upon contact with the subendothelial matrix quench blebbing in favor of a lamellipodial mode of migration.

Significantly, we also show here for the first time that MSC blebs can exert forces on endothelium. Although it remains to be determined whether such forces function to breach the endothelial barrier and initiate transmigration, blebbing activity was well-associated with gap/pore formation, and the initial phase of subendothelial spreading. Thus, it is possible that nonapoptotic blebbing by MSC may function as an alternate to the actin-rich protrusive structures (e.g., lamellipodia, pseudopodia, and invadosomes) that leukocytes use to breach the endothelium. Two recent in vivo [46] and in ex vivo organ culture [14] studies provide support for the physiological relevance of this hypothesis. Specifically, MSCs were found to initiate extravasation by extending "plasmic podia" across the endothelium [46, 14]. Although not characterized in any detail, the fact that these plasmic podia were of identical scale and morphology as the nonapoptotic membrane blebs described herein leads us to speculate that these two structures are one in the same. Finally, it is interesting to note that tumor cell blebs have also been observed in models of tumor extravasation, although their dynamics and functional roles remain to be characterized [33, 47].

Conclusion

In summary, we have performed novel and high-resolution morphological and dynamic characterization of MSC transmigration. In this way, we provide new insights for the cellular processes that mediate MSC transmigration (Fig. 6). Specifically, we show for the first time that in addition to integration, MSC can also transmigrate through discrete gaps and pores by paracellular and transcellular diapedesis processes, partially similar to those used by leukocytes. Additionally, MSC transmigration was strongly associated with nonapoptotic membrane blebbing. This is the first demonstration, to our knowledge, of blebbing by a physiologic cell type during diapedesis.

As discussed above, the in vitro models used in this study are inherently limited with respect to their ability to fully recapitulate the physiologic settings of MSC extravasation. Additionally, our study models a generic inflammatory condition and cannot account for all the heterogeneity that arises in distinct tissues/vascular beds and the diverse setting for inflammation, such as ischemic injury, tissue trauma, and infection. Thus, future studies are needed to critically evaluate and extend the current findings in diverse in vivo models. Elucidating the mechanistic underpinning for MSC diapedesis will be critical to understand MSC recruitment to sites of inflammation in physiological, pathological, and clinical settings.

Acknowledgments

This work was supported by grants from the National Institute of Health (HL097172, HL095722, and DE019191 [J.M.K.] and HL104006 [C.V.C.]), the American Heart Association (0970178N [J.M.K.] and 09SDG2130011 [C.V.C.]), and the Roche Organ Transplant Research Organization (C.V.C.). J.A.A. was supported by the Hugh Hampton Young Memorial Fund and National Science Foundation. Some of the materials used in this work were provided by the Texas A&M Health Science Center College of Medicine Institute for Regenerative Medicine at Scott & White through a grant from NCRR of the NIH, Grant #P40RR017447. We thank Dr. John Greenwood (University College of London, U.K.) for providing the GPNT rat brain MVEC line.

Disclosure of Potential Conflicts of Interest

JMK is a co-owner of Megacell Therapeutics, a company that has an option to license IP generated by JMK. JMK may benefit financially if the IP is licensed and further validated. JMK's interests were reviewed and are subject to a management plan overseen by the Brigham and Women's Hospital and Partners HealthCare in accordance with their conflict of interest policies. All other authors indicate no potential conflicts of interest.

References

1 Ankrum J, Karp JM. Mesenchymal stem cell therapy: Two steps forward, one step back. Trends Mol Med 2009;16:203–209.
2 Karp JM, Teo GSL. Mesenchymal stem cell homing: The devil is in the details. Cell Stem Cell 2009;4:206–216.
3 Kawada H, Fujita J, Kinjo K et al. Nonhematopoietic mesenchymal stem cells can be mobilized and differentiate into cardiomyocytes after myocardial infarction. Blood 2004;104:3581–3587.
4 Quante M, Tu SP, Tomita H et al. Bone marrow-derived myofibroblasts contribute to the mesenchymal stem cell niche and promote tumor growth. Cancer Cell 2011;19:257–272.
5 Taylor HS. Endometrial cells derived from donor stem cells in bone marrow transplant recipients. JAMA 2004;292:81–85.
6 Du H,Taylor HS. Contribution of bone marrow-derived stem cells to endometrium and endometriosis. Stem Cells 2007;25:2082–2086.
7 Wang C-H, Cherng W-J, Yang N-I et al. Late-outgrowth endothelial cells attenuate intimal hyperplasia contributed by MSCs after vascular injury. Arterioscler Thromb Vasc Biol 2008;28:54–60.
8 Ley K, Laudanna C, Cybulsky MI et al. Getting to the site of inflammation: The leukocyte adhesion cascade updated. Nat Rev Immunol 2007;7:678–689.
9 Carman CV. Mechanisms for transcellular diapedesis: Probing and pathfinding by 'invadosome-like protrusions'. J Cell Sci 2009;122:3025–3035.
10 Carman CV. Transmigratory cups and invadosome-like protrusions: New aspects of diapedesis. In: Ley K, ed. Leukocyte Adhesion:

Current Topics in Membranes. Vol 64. Amsterdam: Elsevier, 2009: 297–333.
11 Ruster B, Gottig S, Ludwig RJ et al. Mesenchymal stem cells display coordinated rolling and adhesion behavior on endothelial cells. Blood 2006;108:3938–3944.
12 Segers VFM,Van Riet I,Andries LJ et al. Mesenchymal stem cell adhesion to cardiac microvascular endothelium: Activators and mechanisms. Am J Physiol Heart Circ Physiol 2006;290:H1370–1377.
13 Schmidt A, Ladage D, Steingen C et al. Mesenchymal stem cells transmigrate over the endothelial barrier. Eur J Cell Biol 2006;85: 1179–1188.
14 Steingen C, Breniga F, Baumgartnera L et al. Characterization of key mechanisms in transmigration and invasion of mesenchymal stem cells. J Mol Cell Cardiol 2008;44:1072–1084.
15 Langer HF, Stellos K, Steingen C et al. Platelet derived bFGF mediates vascular integrative mechanisms of mesenchymal stem cells in vitro. J Mol Cell Cardiol 2009;47:315–325.
16 Charras G, Paluch E. Blebs lead the way: How to migrate without lamellipodia. Nat Rev Mol Cell Biol 2008;9:730–736.
17 Fackler OT, Grosse R. Cell motility though plasma membrane blebbing. J Cell Biol 2008;181:879–884.
18 Sahai E, Marshall CJ. Differing modes of tumour cell invasion have distinct requirements for Rho/ROCK signalling and extracellular proteolysis. Nat Cell Biol 2003;5:711–719.
19 Carman CV, Springer TA. A transmigratory cup in leukocyte diapedesis both through individual vascular endothelial cells and between them. J Cell Biol 2004;167:377–388.
20 Sarkar D, Vemula PK, Teo GSL et al. Chemical engineering of mesenchymal stem cells to induce a cell rolling response. Bioconjug Chem 2008;19:2105–2109.
21 Roux F, Couraud P-O. Rat brain endothelial cell lines for the study of blood-brain barrier permeability and transport functions. Cell Mol Neurobiol 2003;25:41–47.
22 Romero IA, Prevost M-C, Perret E et al. Interactions between brain endothelial cells and human T-cell leukemia virus type 1-infected lymphocytes: Mechanisms of viral entry into the central nervous system. J Virol 2000;74:6021–6030.
23 Bernas MJ,Cardoso FL,Daley SK et al. Establishment of primary cultures of human brain microvascular endothelial cells to provide an in vitro cellular model of the blood-brain barrier. Nat Protocols 5:1265–1272.
24 Balda MS, Whitney JA, Flores C et al. Functional dissociation of paracellular permeability and transepithelial electrical resistance and disruption of the apical-basolateral intramembrane diffusion barrier by expression of a mutant tight junction membrane protein. J Cell Biol 1996;134:1031–1049.
25 Carman CV, Jun C-D, Salas A et al. Endothelial cells proactively form microvilli-like membrane projections upon intercellular adhesion molecule 1 engagement of leukocyte LFA-1. J Immunol 2003;171: 6135–6144.
26 Barr VA,Bunnell SC. Interference reflection microscopy. Curr Protoc Cell Biol 2009; Chapter 4:Unit 4 23.
27 Carman CV, Sage PT, Sciuto TE et al. Transcellular diapedesis is initiated by invasive podosomes. Immunity 2007;26:784–797.
28 Wagner W,Horn P,Castoldi M et al. Replicative senescence of mesenchymal stem cells: A continuous and organized process. PLoS One 2008;3:e2213.
29 Abel S, Hundhausen C, Mentlein R et al. The transmembrane CXC-chemokine ligand 16 is induced by IFN-gamma and TNF-alpha and shed by the activity of the disintegrin-like metalloproteinase ADAM10. J Immunol 2004;172:6362–6372.
30 Smith H, Whittal C, Weksler B et al. Chemokines stimulate bidirectional migration of human mesenchymal stem cells across bone marrow endothelial cells. Stem Cells Dev 2012;21:476–486.
31 Barreiro O, Yanez-Mo M, Serrador JM et al. Dynamic interaction of VCAM-1 and ICAM-1 with moesin and ezrin in a novel endothelial docking structure for adherent leukocytes. J Cell Biol 2002;157: 1233–1245.
32 Niessen CM. Tight junctions/adherens junctions: Basic structure and function. J Invest Dermatol;127:2525–2532.
33 Voura EB, Sandig M, Siu C-H. Cell–cell interactions during transendothelial migration of tumor cells. Microsc Res Tech 1998;43: 265–275.
34 Maloney JM, Nikova D, Lautenschlager F et al. Mesenchymal stem cell mechanics from the attached to the suspended state. Biophys J 2010;99:2479–2487.
35 Chamberlain G,Smith H,Rainger GE et al. Mesenchymal stem cells exhibit firm adhesion, crawling, spreading and transmigration across aortic endothelial cells: Effects of chemokines and shear. PLoS One 2011;6:e25663.
36 Thankamony SP, Sackstein R. Enforced hematopoietic cell E- and L-selectin ligand (HCELL) expression primes transendothelial migration of human mesenchymal stem cells. Proc Natl Acad Sci 2011;108:2258–2263.
37 De Becker A, Van Hummelen P, Bakkus M et al. Migration of culture-expanded human mesenchymal stem cells through bone marrow endothelium is regulated by matrix metalloproteinase-2 and tissue inhibitor of metalloproteinase-3. Haematologica 2007;92:440–449.
38 Lozito TP, Tuan RS. Mesenchymal stem cells inhibit both endogenous and exogenous MMPs via secreted TIMPs. J Cell Physiol 2011;226: 385–396.
39 Barreiro O, Zamai M, Yanez-Mo M et al. Endothelial adhesion receptors are recruited to adherent leukocytes by inclusion in preformed tetraspanin nanoplatforms. J Cell Biol 2008;183:527–542.
40 Carman CV. The endothelial cytoskeleton. In: Aird WC, ed. Endothelial Biomedicine. Cambridge: Cambridge University Press, 2007:696–706.
41 Byfield FJ, Reen RK, Shentu T-P et al. Endothelial actin and cell stiffness is modulated by substrate stiffness in 2D and 3D. J Biomech 2009;42:1114–1119.
42 Krishnan R,Klumpers DD,Park CY et al. Substrate stiffening promotes endothelial monolayer disruption through enhanced physical forces. Am J Physiol—Cell Physiol 2010;300:C146–C154.
43 Stroka KM, Aranda-Espinoza H. Endothelial cell substrate stiffness influences neutrophil transmigration via myosin light chain kinase-dependent cell contraction. Blood 2011;118:1632–1640.
44 Lapis K, Paku S, Liotta LA. Endothelialization of embolized tumor cells during metastasis formation. Clin Exp Metastasis 1988;6:73–89.
45 Crissman JD, Hatfield J, Schaldenbrand M, Sloane BF, Honn KV. Arrest and extravasation of B16 amelanotic melanoma in murine lungs. A light and electron microscopic study. Lab Invest 1985;53:470–478.
46 Ghanem A, Steingen C, Brenig F et al. Focused ultrasound-induced stimulation of microbubbles augments site-targeted engraftment of mesenchymal stem cells after acute myocardial infarction. J Mol Cell Cardiol 2009;47:411–418.
47 Estecha A, Sanchez-Martan L, Puig-Kroger A et al. Moesin orchestrates cortical polarity of melanoma tumour cells to initiate 3D invasion. J Cell Sci 2009;122:3492–3501.


See www.StemCells.com for supporting information available online.